A Strong Coupling Model for the Simulation of Magnetomechanical Systems using a Predictor/Multicorrector Algorithm

M. Kaltenbacher, H. Landes, R. Lerch
Department of Electrical Measurement Technology, University of Linz, Altenbergerstr. 69, A-4040 Linz, Austria

Abstract – **A recently developed modeling scheme for the numerical simulation of coupled magnetomechanical systems is presented. The scheme allows the calculation of dynamic rigid motions as well as deformations of magnetic and anti-magnetic materials in a magnetic field. The equations governing the magnetic and mechanical field quantities are solved using a combined Finite-Element/Boundary-Element-Method (FEM-BEM). To circumvent the nonlinear system of equations resulting from a direct coupling of the magnetic and mechanical systems, the calculation of the magnetic forces is based on predictor values of the magnetic quantities. Therewith, a decoupling into a magnetic and mechanical matrix equation can be achieved. To ensure the strong coupling between the magnetic and mechanical quantities, a sophisticated Predictor/Multicorrector Algorithm is used resulting in an efficient iteration between the two matrix equations within a single time step. Computer simulations of an electromagnetic forming system and a magnetomechanical transducer immersed in an acoustic fluid (acoustic power source) show good agreement between simulation results and measured data.**

I. Introduction

In magnetomechanical systems a magnetic material is subject both to rigid motions and to elastic (plastic) deformations, which in turn may strongly influence the magnetic field and thus the magnetic force distribution. Therefore, a modeling scheme must take into account the strong coupling of the magnetic and mechanical field quantities [1], [2].

A typical magnetomechanical system is shown in Fig. 1. When the coil is loaded by an electric current pulse, eddy currents are induced in the metallic cylinder. The interaction between these eddy currents and the magnetic field results in magnetic volume forces acting on the body. Therewith, in the case that the stress within the workpiece exceeds the yield point of the material, the metallic cylinder will experience plastic deformations. These deformations modify the magnetic field and thus the force distribution acting on the magnetic cylinder. To obtain a full description of the dynamic behaviour of the electromagnetic forming system, the following coupling mechanisms have to be considered:

Manuscript received September 23, 1996.
M. Kaltenbacher, e-mail m.kaltenbacher@jk.uni-linz.ac.at, fax 0043-732-2468-10; H. Landes, e-mail h.landes@jk.uni-linz.ac.at; R. Lerch, e-mail r.lerch@jk.uni-linz.ac.at;

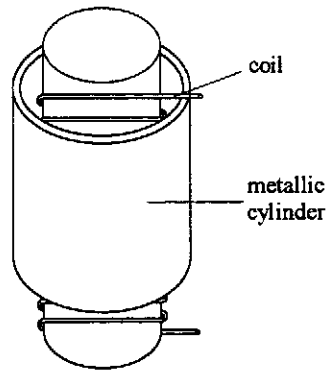

Fig. 1. Electromagnetic forming of a metallic cylinder

- The coupling between the magnetic and mechanical field is due to magnetic volume forces caused by eddy currents in the metallic cylinder and the magnetic field of the coil.
- The resulting plastic deformations (movements) of the metallic cylinder in the magnetic field cause additional eddy currents in the metallic cylinder (motional emf).
- The metallic cylinder changes its geometry significantly during the electromagnetic forming process which in turn strongly influences the magnetic field.

Applying a numerical technique to calculate the quantities of the magnetomechanical system, the following main problems will arise:

- Using a standard finite element code, the moving parts cause mesh distortion and, therefore, may introduce geometric nonlinearities. In addition, if the displacement exceeds the element size, a new meshing of the whole simulation area is required.
- A direct coupling of the magnetic and mechanical quantities leads to a nonlinear system of equations, due to the magnetic force.

- The term of the motional emf leads to numerical difficulties in the partial differential equation describing the magnetic field.

II. Governing Equations

In the case of low frequencies (neglecting displacement current) magnetic systems with stationary and moving parts can be described by the following partial differential equation

$$\nabla \times \left(\frac{1}{\mu}\nabla \times \vec{A}\right) = \vec{J}_e - \gamma\frac{\partial \vec{A}}{\partial t} - \gamma\nabla V + \gamma\vec{v} \times (\nabla \times \vec{A}). \quad (1)$$

In (1) $\vec{A}$ denotes the magnetic vector potential, $\vec{J}_e$ the free current density, μ the permeability , V the scalar electric potential, $\vec{v}$ the velocity and γ the conductivity. The term $\gamma\vec{v} \times (\nabla \times \vec{A})$ expresses the induced eddy current density in an electric conductive body moving with velocity $\vec{v}$ in a magnetic field (motional emf).

In the case of linear elasticity and isotropic materials, the dynamic behaviour of mechanical systems can be described by

$$\frac{E}{2(1+\nu)}\left((\nabla\cdot\nabla)\vec{d} + \frac{1}{1-2\nu}\nabla(\nabla\cdot\vec{d})\right) + \vec{f}_V = \rho\frac{\partial^2\vec{d}}{\partial t^2}, \quad (2)$$

where $\vec{d}$ is the mechanical displacement, $\vec{f}_V$ the volume force, E the modulus of elasticity, ν Poisson's ratio and ρ the density. The magnetic volume force due to a magnetic field of magnetic induction $\vec{B}$ (magnetic field intensity $\vec{H}$) acting on a body with current density $\vec{J}$ is given by

$$\vec{f}_V = \vec{J} \times \vec{B}. \quad (3)$$

To calculate the plastic deformations (electromagnetic forming of an aluminium cylinder, Fig. 1) a visco-plastic model with consolidation is used. The state of stress is represented by a stress tensor with a single component, tangential to the wall of the cylinder and uniform over its surface. Furthermore, no account is taken of the fact that during the forming process the workpiece becomes shorter and its wall thinner. Therewith, the equilibrium equation for the cylinder expanding plastically under an internal pressure is given by

$$P_r = \frac{\sigma e}{r} + \rho e\frac{dv_r}{dt} \quad (4)$$

with e, r and ρ being the thickness, radius and mass density of the workpiece, σ the radial stress, P_r the radial electromagnetic pressure and v_r the radial velocity. Assuming a uniform stress over the surface of the tube, the magnetic pressure is obtained by

$$P_r = \frac{2\pi\int\int f_{Vr} r\,dr\,dz}{2\pi r h}. \quad (5)$$

In (5) h denotes the length of the metallic cylinder and f_{Vr} the radial component of the magnetic volume force $\vec{f}_V$ in (3).

The relation between stress, strain and strain rate has the form [3]:

$$\sigma = \sigma_d + \lambda\varepsilon + \eta\left(\frac{d\varepsilon}{dt}\right)^{\delta}, \quad (6)$$

where σ_d is the yield point, ε the relative strain, $d\varepsilon/dt$ the strain rate, λ the consolidation coefficient, η the coefficient of viscosity and δ a coefficient such that (6) closely approaches the characteristics determined experimentally.

III. FEM-BEM- and Time-Discretization

Applying the FE-formulation to (1) leads to the FE-matrix equation

$$\mathbf{L}\{R\} + \mathbf{P}\{A\} + \tilde{\mathbf{P}}\{Av\} - \tilde{\mathbf{C}}\{q\} = \{Q\} \quad (7)$$

with conductivity matrix $\mathbf{L}$, standard permeability matrix $\mathbf{P}$, permeability matrix $\tilde{\mathbf{P}}$ due to motional emf, coupling matrix $\tilde{\mathbf{C}}$, nodal magnetic vector potentials $\{A\}$, nodal time derivatives of the magnetic vector potential $\{R\}$, nodal normal derivatives of the magnetic vector potential $\{q\}$ and source vector $\{Q\}$.

The boundary element discretization of regions not containing electric currents yields the following BE-matrix equation

$$\mathbf{H}\{A\} - \mathbf{G}\{q\} = \{0\} \quad (8)$$

with the two boundary element matrices $\mathbf{H}$ and $\mathbf{G}$.

The coupling of the finite and boundary elements analogous to [4] leads to the following matrix equation:

$$\begin{pmatrix} \mathbf{L} & \mathbf{P} & \tilde{\mathbf{P}} & -\tilde{\mathbf{C}} \\ \mathbf{0} & \mathbf{H} & \mathbf{0} & -\mathbf{G} \end{pmatrix} \begin{pmatrix} \{R\} \\ \{A\} \\ \{Av\} \\ \{q\} \end{pmatrix} = \begin{pmatrix} \{Q\} \\ \{0\} \end{pmatrix}. \quad (9)$$

Considering dynamic rigid motions of magnetic and antimagnetic materials the matrices $\mathbf{L}$, $\mathbf{P}$ and $\tilde{\mathbf{C}}$ remain constant throughout the whole simulation. This holds true in the case of small deformations (linear elasticity), too. The coordinates of the boundary elements have to be updated according to the mechanical displacements. Therewith, the matrices $\mathbf{H}$ and $\mathbf{G}$ will vary during the simulation, which will be indicated in the following by the letter a. Due to the updating of the coordinates of the boundary

elements, the motional emf is implicitly taken into account and the term $\tilde{\mathbf{P}}\{Av\}$ in (7) vanishes. Therefore (9) reduces to

$$\begin{pmatrix} \mathbf{L} & \mathbf{P} & -\tilde{\mathbf{C}} \\ \mathbf{0} & {}^{a}\mathbf{H} & -{}^{a}\mathbf{G} \end{pmatrix} \begin{pmatrix} \{R\} \\ \{A\} \\ \{q\} \end{pmatrix} = \begin{pmatrix} \{Q\} \\ \{0\} \end{pmatrix} . \quad (10)$$

Applying the FE-formulation to (2) leads to the well-known matrix equation for the mechanical quantities

$$\mathbf{M}\{a\} + \mathbf{C}\{v\} + \mathbf{K}\{d\} - \{F(A, \partial A/\partial t, d) = \{0\} \quad (11)$$

with mass matrix $\mathbf{M}$, damping matrix $\mathbf{C}$, stiffness matrix $\mathbf{K}$, force vector $\{F\}$ including the nonlinear term, nodal accelerations $\{a\}$, nodal velocities $\{v\}$ and nodal displacements $\{d\}$.

For the time discretization of (10) the *generalized trapezoidal method* [5] is used, which has the following predictor/corrector form:

Predictor:

$$\{\tilde{A}\} = \{A\}^n + \Delta t(1-\gamma_P)\{R\}^n \quad (12)$$
$$\{\tilde{q}\} = \{q\}^n + \Delta t(1-\gamma_P)\{r\}^n \quad (13)$$

Equation:

$$\begin{pmatrix} \mathbf{L}^* & \tilde{\mathbf{C}}^* \\ {}^{a}\mathbf{H}^* & {}^{a}\mathbf{G}^* \end{pmatrix} \begin{pmatrix} \{R\}^{n+1} \\ \{r\}^{n+1} \end{pmatrix} = \begin{pmatrix} \{Q\}^{n+1} \\ \{0\} \end{pmatrix} - \begin{pmatrix} \mathbf{P}\{\tilde{A}\} - \tilde{\mathbf{C}}\{\tilde{q}\} \\ {}^{a}\mathbf{H}\{\tilde{A}\} - {}^{a}\mathbf{G}\{\tilde{q}\} \end{pmatrix} \quad (14)$$

$$\mathbf{L}^* = \mathbf{L} + \gamma_P \Delta t \mathbf{P} \quad , \quad \tilde{\mathbf{C}}^* = -\gamma_P \Delta t \tilde{\mathbf{C}} \quad (15)$$
$${}^{a}\mathbf{H}^* = \gamma_P \Delta t \, {}^{a}\mathbf{H} \quad , \quad {}^{a}\mathbf{G}^* = -\gamma_P \Delta t \, {}^{a}\mathbf{G} . \quad (16)$$

Corrector:

$$\{A\}^{n+1} = \{\tilde{A}\} + \gamma_P \Delta t\{R\}^{n+1} \quad (17)$$
$$\{q\}^{n+1} = \{\tilde{q}\} + \gamma_P \Delta t\{r\}^{n+1} \quad (18)$$

In (12) - (18) n denotes the current step, Δt the time step and γ_P the integration parameter.

Using the *Newmark Method* [5] with the two integration parameters β and γ_H for the time discretization of (11) the following predictor/corrector algorithm is obtained:

Predictor:

$$\{\tilde{d}\} = \{d\}^n + \Delta t\{v\}^n + \frac{1}{2}\Delta t^2(1-2\beta)\{a\}^n \quad (19)$$
$$\{\tilde{v}\} = \{v\}^n + (1-\gamma_H)\Delta t\{a\}^n \quad (20)$$

Equation:

$$\mathbf{M}^*\{a\}^{n+1} = \{F(A^{n+1}, R^{n+1}, d^{n+1})\} - \mathbf{K}\{\tilde{d}\} - \mathbf{C}\{\tilde{v}\}$$
$$\mathbf{M}^* = \mathbf{M} + \gamma_H \Delta t\mathbf{C} + \beta\Delta t^2\mathbf{K} \quad (21)$$

Corrector:

$$\{d\}^{n+1} = \{\tilde{d}\} + \beta\Delta t^2\{a\}^{n+1} \quad (22)$$
$$\{v\}^{n+1} = \{\tilde{v}\} + \gamma_H\Delta t\{a\}^{n+1} \quad (23)$$

IV. Predictor/Multicorrector Algorithm

The direct coupling of (14) and (21) leads to a nonlinear and unsymmetric system of equations. Using predictor values for the calculation of the magnetic volume force, a decoupling into a magnetic and mechanical matrix equation can be achieved. To ensure the strong coupling between the magnetic and mechanical quantities the following Predictor/Multicorrector Algorithm is used:

STEP 1: Set the iteration counter i to zero and define the predictor values as following:
Magnetic quantities:

$$\begin{aligned} {}^{i}\{\tilde{A}\} &= \{A\}^n + (1-\gamma_P)\Delta t\{R\}^n \\ {}^{i}\{\tilde{q}\} &= \{q\}^n + (1-\gamma_P)\Delta t\{r\}^n \\ \{\tilde{R}\} &= \{\tilde{r}\} = \{0\} \end{aligned} \quad (24)$$

Mechanical quantities:

$$\begin{aligned} {}^{i}\{\tilde{d}\} &= \{d\}^n + \Delta t\{v\}^n + \tfrac{1}{2}(1-2\beta)\Delta t^2\{a\}^n \\ {}^{i}\{\tilde{v}\} &= \{v\}^n + (1-\gamma_H)\Delta t\{a\}^n \\ \{\tilde{a}\} &= \{0\} \end{aligned} \quad (25)$$

STEP 2: Solve the matrix equation:

$$\begin{pmatrix} \mathbf{L}^* & \tilde{\mathbf{C}} & \mathbf{0} \\ {}^{a}\mathbf{H}^* & {}^{a}\mathbf{G}^* & \mathbf{0} \\ \mathbf{0} & \mathbf{0} & \mathbf{M}^* \end{pmatrix} \begin{pmatrix} \{\Delta R\} \\ \{\Delta r\} \\ \{\Delta a\} \end{pmatrix} = \begin{pmatrix} {}^{i}\{\Delta Q_1\} \\ {}^{i}\{\Delta Q_2\} \\ {}^{i}\{\Delta Q_3\} \end{pmatrix} \quad (26)$$

$$\begin{aligned} {}^{i}\{\Delta Q_1\} &= \{Q\}^{n+1} - \mathbf{P}\,{}^{i}\{\tilde{A}\} + \tilde{\mathbf{C}}\,{}^{i}\{\tilde{q}\} - \mathbf{L}\,{}^{i}\{\tilde{R}\} \\ &\quad + \tilde{\mathbf{C}}\,{}^{i}\{\tilde{r}\} \\ {}^{i}\{\Delta Q_2\} &= {}^{a}\mathbf{G}\,{}^{i}\{\tilde{q}\} - {}^{a}\mathbf{H}\,{}^{i}\{\tilde{A}\} - {}^{a}\mathbf{H}\,{}^{i}\{\tilde{R}\} + {}^{a}\mathbf{G}\,{}^{i}\{\tilde{r}\} \\ {}^{i}\{\Delta Q_3\} &= \{F({}^{i}\tilde{A}, {}^{i}\tilde{R}, {}^{i}\tilde{d})\} - \mathbf{K}\,{}^{i}\{\tilde{d}\} - \mathbf{C}\,{}^{i}\{\tilde{v}\} - \mathbf{M}\,{}^{i}\{\tilde{a}\} \end{aligned}$$

STEP 3: Perform the corrector phase (predictor update)
Magnetic quantities:

$$\begin{aligned} {}^{i+1}\{\tilde{A}\} &= {}^{i}\{\tilde{A}\} + \gamma_P\Delta t\{\Delta R\} \\ {}^{i+1}\{\tilde{q}\} &= {}^{i}\{\tilde{q}\} + \gamma_P\Delta t\{\Delta r\} \\ {}^{i+1}\{\tilde{R}\} &= {}^{i}\{\tilde{R}\} + \{\Delta R\} \\ {}^{i+1}\{\tilde{r}\} &= {}^{i}\{\tilde{r}\} + \{\Delta r\} \end{aligned} \quad (27)$$

Mechanical quantities:

$$\begin{aligned} {}^{i+1}\{\tilde{d}\} &= {}^{i}\{\tilde{d}\} + \beta\Delta t^2\{\Delta a\} \\ {}^{i+1}\{\tilde{v}\} &= {}^{i}\{\tilde{v}\} + \gamma_H\Delta t\{\Delta a\} \\ {}^{i+1}\{\tilde{a}\} &= {}^{i}\{\tilde{a}\} + \{\Delta a\} \end{aligned} \quad (28)$$

STEP 4: Next iteration: go to STEP 2
STEP 5: Solution for step (n+1)

In (24) - (28) i denotes the iteration counter, ${}^{i}\{\Delta Q_1\}$, ${}^{i}\{\Delta Q_3\}$ and ${}^{i}\{\Delta Q_3\}$ the residual vectors of the right hand side for step $(n+1)$ and iteration i and $\{\Delta R\}$, $\{\Delta r\}$ and

$\{\Delta a\}$ the solution vectors of the current iteration. Compared to a standard iteration algorithm the main difference consists in the fact, that the right hand side vectors of iteration i are calculated by the difference of the source vectors and the solution of iteration i. Therewith, the residual of the right hand side vectors as well as the solution vectors converge to zero by increasing number of iterations and thus are used for stopping the iteration. After the iterative phase has terminated, the solution is defined by the last iterates and the algorithm proceeds to the next time step.

Iterative solvers - GMRES (generalized minimum residual) and CGS (conjugate gradient squared) - have been adapted to solve (26) in a very fast way.

V. Application

A. Electromagnetic Forming System

The FEM-BEM discretization of the electromagnetic forming system (Fig. 1) is shown in Fig. 2. The boundary elements, describing the calculation area (up to infinity) surrounding the coil and metallic cylinder, guarantee the coupling of the physical quantities between the stationary part (coil) and moving part (metallic cylinder). Fig. 3 shows the measured current loading the coil, which consists of 12 turns. The magnetic pressure P_r, resulting form the interaction of the magnetic field and the eddy currents in the metallic cylinder, is calculated by (5). Combining (4) and (6) the differential equation is achieved for computing the plastic deformation in radial direction, which has been coupled to the magnetic equation analogous to the case of linear elasticity. The metallic cylinder is made of aluminium with a yield point of 76 N/mm^2 (plastic pressure of 5.067 N/mm^2) [6]. Fig. (4) shows the calculated and form measuring the magnetic induction estimated magnetic pressure. The final measured displacement and the computed displacement as well as velocity are shown in Fig. 5.

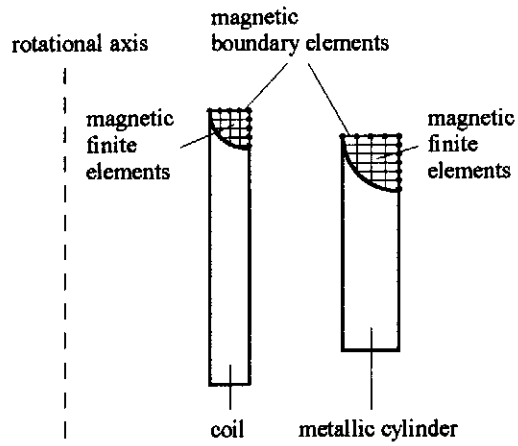

Fig. 2. FEM-BEM discretization of the electromagnetic forming system

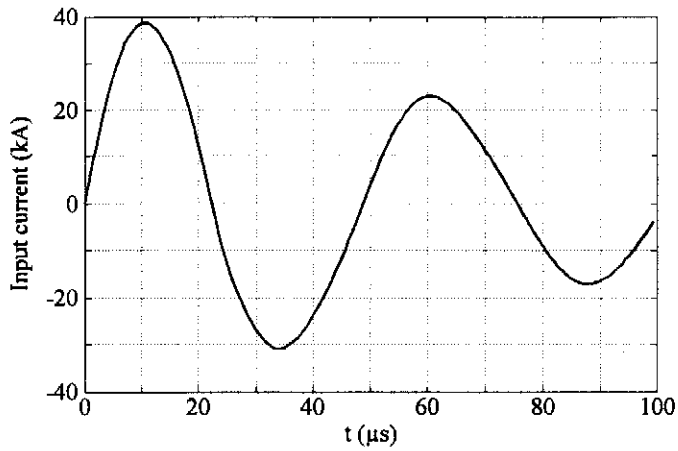

Fig. 3. Measured electric current loading the coil [6]

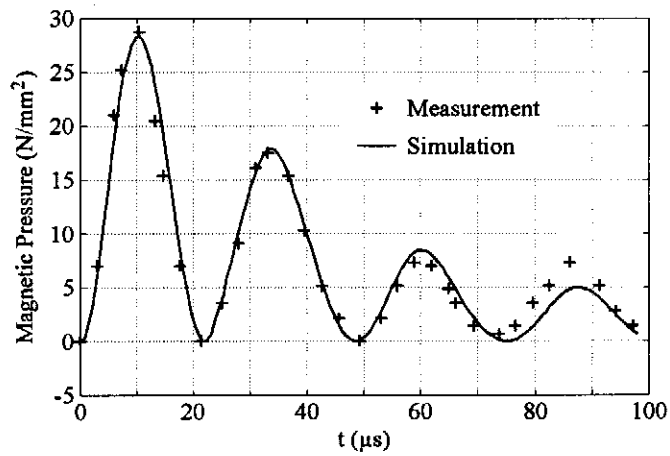

Fig. 4. Measured (estimated by measured magnetic induction [6]) and computed magnetic pressure

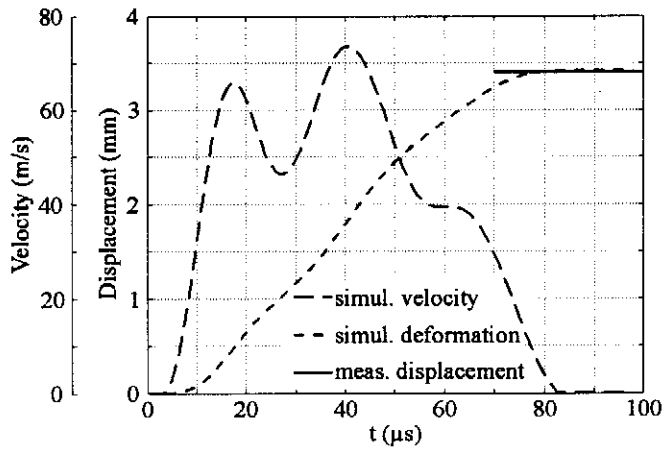

Fig. 5. Measured final displacement [6] and computed displacement as well as velocity

B. Acoustic power source

The acoustic power source (Fig. 6) was optimized to generate high-intensive mechanical pulses for the non-

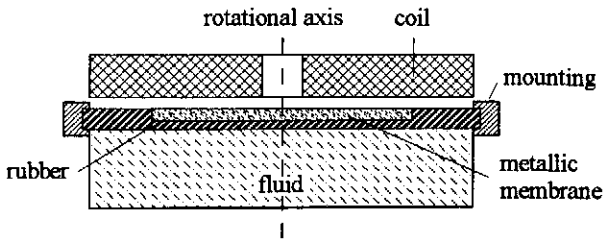

Fig. 6. Schematic of an acoustic power source

invasive destruction of concrements in human kidneys and urinary tract. When the slab coil is loaded by an electric current pulse, eddy currents are induced in the metallic membrane. The interaction between the eddy currents in the metallic membrane and the magnetic field results in a magnetic volume force acting on the membrane. Therewith, the metallic membrane-rubber structure is deformed and an acoustic pulse is radiated into the surrounding medium. The propagation of acoustic waves in non-viscous media is completely described by the scalar acoustic potential ψ, which leads to the linear wave equation [7]. The deformed structure with mechanical stresses displayed by a grey scale is presented in Fig. 7. Near the axis, the magnetic field in contrast to the off-axis region causes only very small forces on the structure. Therefore, the metallic membrane-rubber structure experiences only small accelerations but large deformations and mechanical stresses in this region. Fig. 8 shows measured [8] and simulated displacements of the metallic membrane-rubber structure in the center at different times.

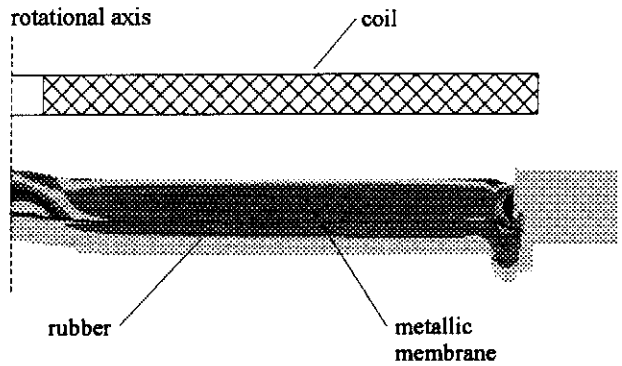

Fig. 7. Deformed metallic membrane-rubber structure with mechanical stresses coded by a grey scale

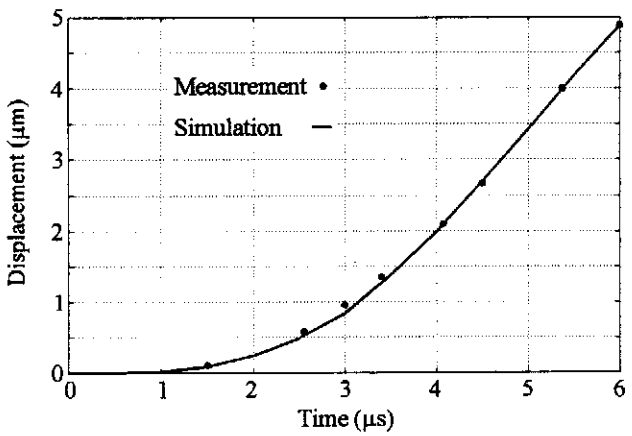

Fig. 8. Measured and simulated displacements of the metallic membrane-rubber structure in the center at different times

VI. Conclusion

A new coupled model for the numerical calculation of magnetomechanical systems has been introduced. Therewith, the complex interaction of magnetic and mechanical fields can be studied. The presented calculation scheme has been applied to the numerical simulation of an electromagnetic forming system and a magnetomechanical transducer immersed in an acoustic fluid. The calculated and measured data are in good agreement.

References

[1] Z. Ren, B. Ionescu, M. Besbes, A. Razek, "Calculation of Mechanical Deformation of Magnetic Materials in Electromagnetic Devices ", IEEE Trans. of Magnetics, vol. 31, No. 3, May 1995, pp. 1813-1816

[2] J.R. Bauer, J.J. Ruehl, M.A. Juds, M.J. VanderHeiden, and A.A. Arkadan, "Dynamic stress in magnetic actuator computed by coupling structural and electromagnetic finite elements ", *IEEE Trans. Magnetics*, vol. 32, May 1996, pp. 1046-1049

[3] B. Bendjima, K.Srairi and M. Féliachi, "A Coupling Model for Analysing Dynamical Behaviours of an Electromagnetic Forming System ", *IEEE CEFC'96* , Okayama, Japan

[4] M. Kaltenbacher, "*Numerische Simulation magnetomechanischer Transducer mit Fluidankopplung*", Ph.D. Thesis, April 1995

[5] T.J.R. Hughes, "*The Finite Element Method* ", New Jersey Prentice-Hall, 1987

[6] C. Fluerasu, "Electromagnetic forming of tubular conductors", *Rev. Roum. Sci. Tech.-Electrotechn. et Energ.*, 15, 3, Bucarest, 1970, pp. 475-488

[7] M. Kaltenbacher, H. Landes, R. Lerch, "An Efficient Calculation Scheme for the Numerical Simulation of Coupled Magnetomechanical Systems", *IEEE CEFC'96*, Okayama, Japan

[8] G. Buchholz, M. Mahler, H. Borner, J. Villain, "Impulsholographie zum Messen von Verformungen an Membranen", *Feinwerktechnik & Messtechnik*, Heft 99, pp. 41-45, 1991